Nanoscale

Accepted Manuscript

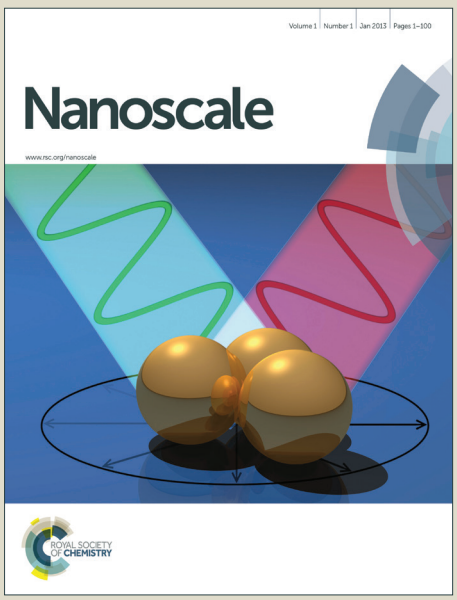

ROYAL SOCIETY OF CHEMISTRY

www.rsc.org/nanoscale

Cite this: DOI: 10.1039/c0xx00000x

www.rsc.org/xxxxxx

ARTICLE TYPE

Two-dimensional Au lattices featuring unique carrier transport preference and wide forbidden gap

Chunmiao Zhang, Yaping Wu*, Yinghui Zhou*, Na Gao, Fei Guo, Xiaohang Chen, Baofeng Jiang, Wei Hu & Junyong Kang*

Received (in XXX, XXX) Xth XXXXXXXXX 20XX, Accepted Xth XXXXXXXXX 20XX
DOI: 10.1039/b000000x

Large-scale 2D Au lattices with honeycomb structure are fabricated on Si(111)-7×7 surface at room temperature. The growth rhythm investigated by reflection high-energy electron diffraction and *in situ* scanning tunneling microscopy indicates that the 2D Au lattices compose two interfacial distinct layers which are completely formed one after another with a close-packed structure. A unique wide forbidden gap of 4.1 eV is measured around the Fermi level of the 2D Au lattices by scanning tunneling spectroscopy. Bias-dependent STM images and theoretical simulations suggest that the in-plane quantum coupling and carrier transport behavior are responsible for the novel electronic properties. Aside from local electronic states, the electronic structures of 2D Au lattices are further modulated by the carrier transport preference that is determined by carrier energy and symmetry of 2D lattices. These findings will provide some references for the controlled fabrication and for routing the carrier transport behavior of low-dimensional metal structures.

Introduction

Two-dimensional (2D) nanostructures have attracted considerable interests in the field of optics, electronics, and magnetism.[1-9] Rich phenomena, such as surface plasmon,[4,5] superconductivity,[6] topological surface states,[7] Kondo effect,[8] and magnetic order in frustrated two-dimensional atom lattices,[9] have made these structures promising candidates for next-generation nanodevices. Particularly, noble metal 2D systems have aroused wide attentions because of their good conductivity and stability in nanoelectronic and catalytic engineering. Since the mature application of Si-based devices, design and fabrication of 2D lattices on Si substrate becomes a new inspiring field. Taking advantage of the periodic Si(111)-7×7 surface, numerous studies have successfully realized the self-organized growth of identically sized nanocluster arrays on many metals, such as Al, Ga, In,[10] Zn,[11] and Au.[12] Based on the highly ordered clusters on Si(111)-7×7 surface, if some additional nanostructures with strict periodic distributions can be further established, the ultrathin metal lattices with enhanced 2D in-plane coupling properties may be obtained. However, compared with the cluster arrays, the confinement effect from the natural 7×7 template is weakened with increasing metal coverage. As a result, building long-range ordered 2D lattices on the Si(111)-7×7 surface is still a challenge. The atomic structure should be well controlled and the growth mechanism should be understood to develop a reproducible growth method.

Due to the broken symmetry in the vertical direction, the 2D systems usually possess unique electronic properties in plane. Raza *et al*. have reported the transport behavior on Si(001)-(2×1) surface with asymmetric dimer reconstruction,[13] and Yamazaki *et al*. have reported the temperature-dependent electrical conduction on various Au/Si(111) surface superstructures.[14] Compared with these systems, the Si(111)-7×7 surface has a relatively longer lattice period. According to the Lindemann criterion $\Delta L = (\langle u_n^2 \rangle)^{1/2}/a$ (where $(\langle u_n^2 \rangle)^{1/2}$ is the root-mean-square displacement fluctuations of an atom, and a is the lattice constant of the crystal),[15] the 2D structure with longer lattice period has smaller displacement fluctuations and larger stable scale. Therefore, it is potentially expected to achieve the room temperature (RT)-stable 2D lattices on Si(111)-7×7 surface. This provides strong motivation to develop an effective growth method and investigate the electronic structures, especially the transport properties of such 2D systems. Furthermore, it is interesting to develop a way to confine, control, and route the electron transport in the 2D lattices, which generally determines the way that 2D devices behave on the atomic scales, similar to the light in photonic crystals with photonic band gap, and may further lead to new concepts and applications in physics.[16,17]

In this work, long-range ordered 2D Au lattices with honeycomb structure are fabricated, and the atomic structure is investigated by means of scanning tunneling microscopy (STM) and reflection high-energy electron diffraction (RHEED). The current–voltage (I–V) properties are studied through scanning tunneling spectroscopy (STS), which reveal a wide energy gap

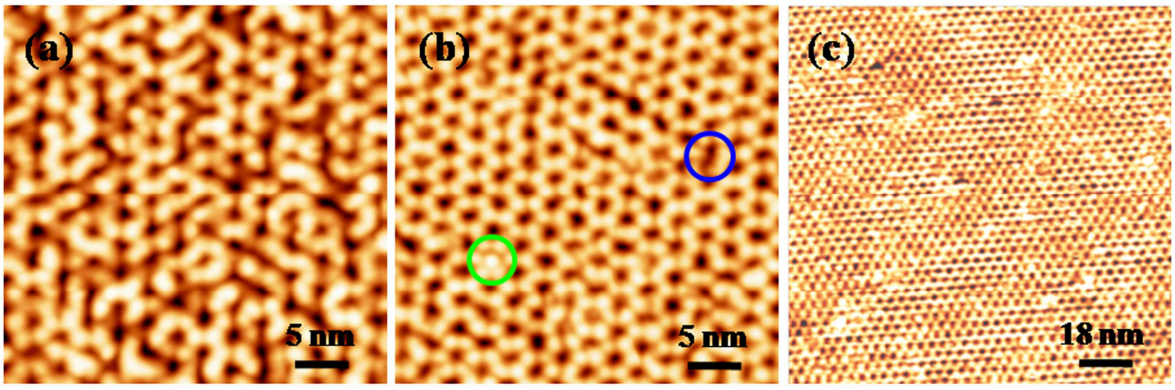

Fig. 1 Topographic STM images of deposition (a) 0.4 ML (25×25 nm^2, +3.5 V, 0.2 nA), (b) 0.8 ML (25×25 nm^2, +3.0 V, 0.2 nA) Au atoms on Si(111)-7×7 surface, respectively. The blue and green circles represent two types of defects on the structure. (c) Large-scale STM image of 2D Au lattices (90×90 nm^2, +3.0 V, 0.2 nA).

around the Fermi level. Bias-dependent STM images show unique quantum coupling effect within the 2D Au lattices, which may be closely related to the in-plane carrier transport behavior. Moreover, finite-difference time-domain simulations are performed to study the transport properties. The results suggest that the wide forbbiden gap is mostly induced by the energy preference of carriers transport in this special 2D structure.

Experimental

The experiments were performed with an Omicron (Germany Multiprobe Compact +2) scanning tunneling microscope operated in ultra-high-vacuum (base pressure of approximately 2.0×10^{-10} mbar). Well-established flash procedures were carried out on *p*-type Si(111) sample to attain an atomically clean Si(111)-7×7 surface. High-purity Au (99.9999%) evaporated from a tantalum boat was deposited onto the Si(111)-7×7 surface at RT at a rate of approximately 0.02 ML/min (1 ML = 7.84×10^{14} Au atoms/cm^2). Low-temperature annealing (~150 °C) was performed to achieve the stable surface. The Au coverage of approximately 0.2, 0.4, and 0.8 ML was obtained by controlling the deposition time. Electrochemically etched tungsten tip was used for the STM scanning to study the surface morphology. All STM images were conducted in the constant-current mode at RT. The electronic structures were characterized by using the STS with a tunneling current of 0.2 nA. The lattice structures were analyzed using an STAIB RHEED with a 15 keV electron energy and an incidence angle $\psi = 1°– 3°$ to the surface.

Results and discussions

Fabrication of 2D Au lattices

2D Au lattices were fabricated by carefully controlling the deposition of Au atoms on the natural template of Si(111)-7×7 surface, and the evolution of the surface morphology at different Au coverage was investigated by STM. Referring to our previous work,[12,18] identically-sized Au clusters have been obtained on the surface after the deposition of 0.2 ML Au atoms. As the Au coverage is increased to 0.4 ML, the original Au clusters further grow (designated as 1L Au-Si clusters) and uniformly coalesce into a honeycomb structure distributing over the Si surface, as shown in Fig. 1(a). As the Au coverage is further increased to 0.8 ML, a highly ordered network structure (bright protrusions, designated as 2L Au structure) with similar symmetry is observed on the surface, as shown in Fig. 1(b). The distance between adjacent corner holes is approximately 2.7 nm, consistent to the periodicity of the Si(111)-7×7 surface. Compared with the honeycomb structure in Fig. 1(a), the network is more compact and exhibits higher contrast. On the ordered network structure, two typical defects can be observed. The one indicated by the blue cycle in Fig. 1(b) is probably induced by the imperfect Si(111)-7×7 substrate, which can lead to the dislocation of the adsorbed Au atoms on top. The second defect type denoted by the green cycle is mostly induced by the slightly redundant deposited Au atoms after the formation of 2D Au lattices, which further fill the corner hole of Si(111)-7×7 substrate. This structure is found globally on the surface as shown in the large-scale STM image in Fig. 1(c), suggesting the successful establishment of long-range ordered 2D Au lattices. The morphology of such artificial 2D lattices remains unchanged after annealing at ~300 °C, indicating good thermal stability.

The atomic configuration of 2D Au lattices

To investigate the atomic configuration of Au lattices and understand the interaction between Au and Si substrates, RHEED images of 0.2, 0.4, and 0.8 ML Au-covered surfaces were obtained and compared with clean Si(111)-7×7 surface, as seen in Fig. 2(a1) to 2(d1) (more clear and enlarged images are further provided in the supporting information S1). Corresponding high-resolution STM images and possible structural models are schematically depicted in Fig. 2(a2) to 2(d2). The deposition of 0.2 ML Au atoms leads to the generation of triangular clusters inside the half unit cells (HUCs), whose configuration was determined as Au_6Si_3 in our previous work.[12] The distribution of the RHEED pattern in Fig. 2(b1) is similar to that of the original Si(111)-7×7 surface in Fig. 2(a1), except for some intensity differences. Detailed inspection reveals that most of the diffraction spots from the substrate are weakened, while the intensity of spots (-2/7, 3/7), (3/7, -2/7), (0, 1/7), (1/7, 0), (0, 4/7), and (4/7, 0) is enhanced, as indicated by the yellow arrows. Such an evolution of the diffraction pattern reflects the structural

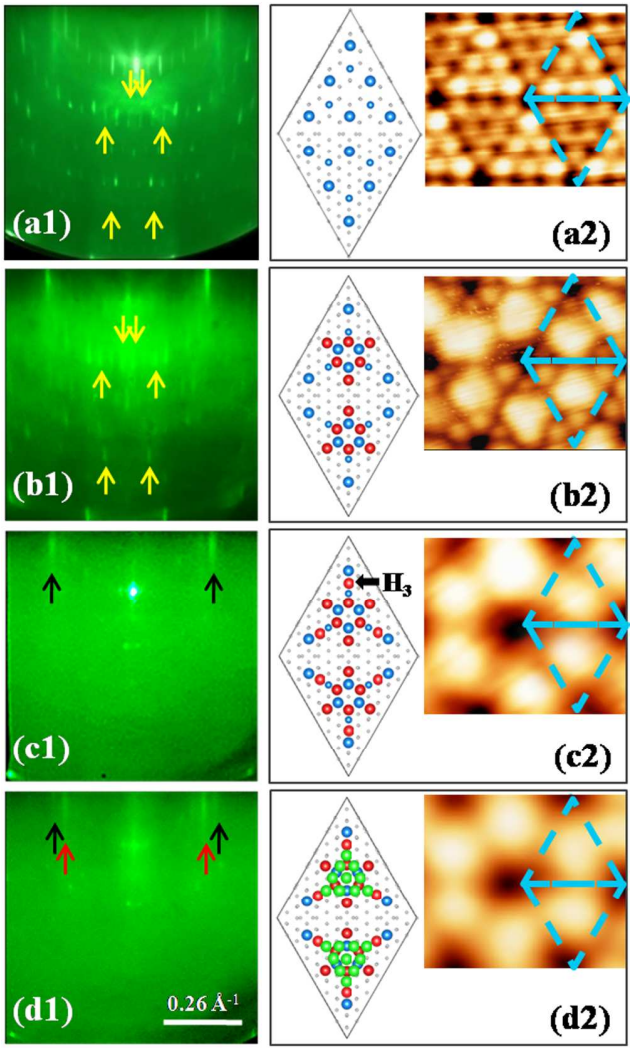

Fig. 2 RHEED patterns for the clean Si(111)-7×7 surface (a1), and that with the deposition of 0.2 ML (b1), 0.4 ML(c1), and 0.8 ML (d1) Au atoms. A scale bar to show the dimension of reciprocal space is indicated in (d1). The incident beam (15 KeV) is parallel to the <1 1 -2> orientation of Si substrate. The yellow, black, and red arrows indicate the intensity evolution of the diffraction spots after the Au deposition. (a2), (b2), (c2) and (d2) are the corresponding structural models and STM images. The blue triangles in STM images indicate the 7×7 unit cells. All STM images are 4.8×5.6 nm^2 in size and taken at 0.2 nA with the bias voltage: (a2) -1.5 V, (b2) -1.5 V, (c2) 3.5 V, and (d2) 3.0 V. The small blue balls, large blue balls, red balls, and green balls represent the Si rest atoms, Si adatoms, Au atoms of 1L Au-Si clusters (0.4 ML deposition), and 2L Au clusters (additional 0.4 ML depositions), respectively.

feature of the surface magic clusters, similar to the phenomenon observed by Chang *et al*. in Ga_6Si_3 clusters on Si(111)-7×7.[19] The intensity of the RHEED pattern is gradually decreased as the Au coverage is further increased. For 0.4 ML deposition, the original clusters turn into large bright protrusions with round shape, and the three surrounded Si corner adatoms are invisible, as shown in the right panel of Fig. 2(c2). Our first-principles calculations indicate that after the occupation of Au_6Si_3 clusters in all HUCs, additional Au atom will prefer to locate on the H_3 site near Si corner adatom (the calculation details are explained in supporting information S2). The Au atom on H_3 site may interact with both the Au_6Si_3 cluster and Si corner adatom, resulting in the electronic-state coupling among them. That may be the reason for the disappearance of the three Si corner adatoms and the enlargement of the 1L Au-Si cluster (Fig. 2(d2)). By further calculating the numbers of deposited Au atoms, we speculate that approximately three additional Au atoms are further adsorbed in each HUC on the H_3 site after all HUCs are covered by the Au_6Si_3 clusters (red atoms in the left panel of Fig. 2(c2)). The RHEED diffraction pattern from the 7×7 surface almost disappears, except for the spots (1, -1) and (-1, 1) marked by the black arrows and the residual diffraction spots at the bottom. This result indicates that the 7×7 surface is covered completely by the honeycomb Au–Si structure. As the Au coverage is further increased to 0.8 ML, the 2D Au lattices are formed. The original diffraction pattern in RHEED image is almost invisible, accompanied by the appearance of two new sharp diffraction streaks adjacent to the original spots (1, -1) and (-1, 1), as indicated by the red arrows in Fig. 2(d1). The diffraction streaks obviously come from the newly formed 2D Au lattices. Detailed measurement of the spacing for the two diffraction streaks shows the relationship of the reciprocal lattices between Au g_{Au} and the Si(111) surface g_{Si}: $g_{Au} = 5g_{Si}/6$. From this equation, the lattice constant within the 2D Au structure is estimated to be 4.6 Å, corresponding to the <1 1 -2> direction of close-packed Au (111) surface (approximately 5.0 Å). The small deviation may be induced by the compressive stress from the Si substrate. Adsorption energy of one 2L Au atom was also calculated to confirm the structural stability on two possible location sites (the calculation details are shown in supporting information S2). The results suggest that, based on the 1L Au-Si surface, additional Au atoms prefer to locate directly on top of the 1L Au-Si clusters rather than occupy the top of dimer site. Combining these theoretical and experimental results, we deduce a possible growth mode of the 2L Au structure: due to the weaker interaction from the substrate, the 2L Au atoms tend to construct with the hexagonal close-packed structure on the 1L Au-Si surface;[12] furthermore, the arrangement of Au and Si atoms of 1L Au-Si surface may serve as a beneficial template for the close-packed configuration. Therefore, the Au atoms are close-packed locating on top of 1L Au-Si clusters, forming an additional Au layer (left panel of Fig. 2(d2)). Unlike the formation of general metal clusters, the growth for the interfacial distinct 1L and 2L Au layers is of special interest that the two layers are completed formed one after another without intergrowth. Such integrated Au network exhibits typical 2D characteristic, which may possess unique electronic properties.

Electronic structures and unique transport properties of 2D Au lattices

To study the electronic structures of the 2D Au lattices, the I–V measurements were performed on the Au network as well as the underlying 1L Au-Si cluster. For validation, we ensured that atomic resolution STM images were acquired during the STS measurements. Fig. 3(a) and 3(b) display the I–V curves measured at the 1L Au-Si and 2L Au structures, respectively, and the normalized numerical differential conductance ((dI/dV)/(I/V)) is plotted correspondingly in Fig. 3(c) and 3(d).[20] The tunneling spectra from the 1L Au-Si clusters on Si HUCs show an energy gap of about 1.0 eV around the Fermi level, indicating a semiconductor characteristic. Compared with the clean Si(111)-

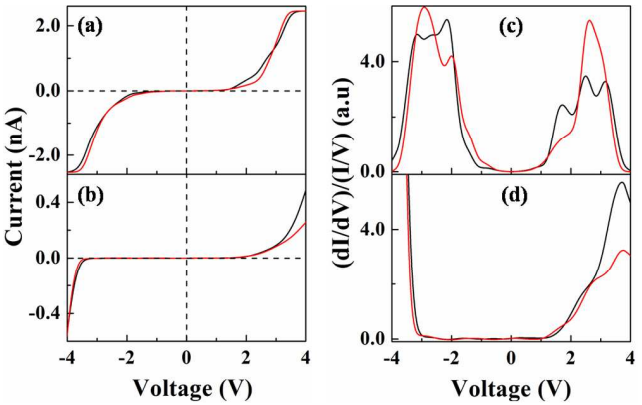

Fig. 3 I–V curves obtained from the (a) 1L Au-Si cluster and (b) 2L Au cluster on the Si(111)-7×7 surface. The black curves are taken at the clusters on the FHUC and the red ones on the UHUC according to 7×7 surface. All the tunneling currents are obtained at a tunneling current of 0.2 nA. (c) And (d), the corresponding normalized numerical differential curves.

7×7 surface, typical surface states within 0.6 V disappear, which can be attributed to the saturation of the dangling bond states on the Si(111)-7×7 surface.[18] In addition, 1L Au-Si clusters on both unfaulted and faulted HUCs exhibit extra seven surface states located at energy levels -3.1, -2.6, -2.0, and -1.5 V below the Fermi level and +1.7, +2.5, and +3.1 V above the Fermi level. The different magnitudes of electronic states between these two curves may result from the differing interaction between 1L Au-Si clusters with the two types of HUCs. In comparison with 1L Au-Si clusters, the tunneling current of the 2L Au network is extremely small at the voltage range of -3.0 to +1.1 V, exhibiting a wide energy gap up to 4.1 eV and a strongly asymmetric electronic structures around the Fermi level.[21,22] The surface states at +1.7 and +2.5 V are seriously suppressed, whereas an additional state is visible at +3.8 V above the Fermi level. In the negative bias voltage region, the surface states that observed at 1L Au-Si clusters almost disappear.

A series of filled- and empty-state STM images were taken at different bias voltages to further reveal the relationship between the electronic properties and surface structures, as shown in Fig. 4. For obtaining these images, the same W tip was used. When the tip was cycled between various voltages, the same result could be reproduced. At the bias voltage of +3.0 V, the STM image in Fig. 4(a) exhibits the ordered honeycomb structure consisting of an array of large bright protrusions whose lateral size and nearest-neighbor spacing were measured to be about 1.0 and 1.5 nm, respectively. Along the $<1\ 1\ -2>_{Si}$ direction, two bright protrusions were found distributed between the corner holes. The protrusions correspond to the surface regions with large tunneling current, rendering as peaks in the height profile (Fig. 4(b)), as denoted by the blue triangles. As the bias voltage is decreased to +2.5 V, the protrusions in HUCs significantly fade out, whereas the dimer sites between HUCs become brighter than the surrounding area and exhibit a Kagome-like morphology.[23] Seemingly, the honeycomb structure observed at +3.0 V rotates approximately 30° around its adjacent corner holes, as indicated by the blue and red hexagons in the inset of Fig. 4(a). Correspondingly, the height profiles indicate that the tunneling current of the dimer sites is relatively raised, whereas that of the protrusions in HUCs is seriously suppressed. In general, the STM images of the isolated clusters are considered to be originated from the surface local density of states (LDOS). However, the tunneling current in the 2D lattices is related not only to LDOS but also to the current spreading within the lattices, *i.e.*, carrier transport and coupling. As mentioned above, no actual Au atoms are adsorbed on the dimer rows of the Si(111)-7×7 substrate. And, the adjacent 2L clusters in 2D Au lattices have a center-to-center distance of about 1.5 nm, which would induce the overlap of the wave function and thus the coupling effects within the lattices.[24] In this way, carriers can transfer between the 2L Au clusters and distribute on the dimer sites that are probed as bright protrusions in the STM images. Thus, the Kagome-like lattices observed at +2.5 V may originate from the rearrangement of electrons in the 2D Au lattices rather than the geometric morphology of the surface. The protrusions in the Kagome-like lattices are smaller, darker, and less ordered compared with those at +3.0 V, because the coupling of wave functions is sensitive to the surface defects and surrounding environments. Closely observation suggests that the Kagome-like structure is a multiple connectivity system having the nested sixfold and threefold symmetric lattices. Such coupling effect provides more transport routes that will distinctly enhance its in-plane transport for the carriers, which has not been found in any metal cluster array or other 2D systems before.

Further decrease the bias voltage to +1.5 V (or lower) results in contrast difference on the HUCs and indistinguishable dimer sites. The height profile is significantly decreased and shows irregular distribution without obvious preference. When the bias voltage is varied to the negative region, as shown for -2.5 V, the contrast on the HUCs and the dimer sites also exhibit irregular distribution, similar with that at the low positive bias voltage below +1.5 V. From the STS results in Fig. 3(b), the tunneling current of 2D Au lattices is rather weak at the bias voltages of +1.5 V and -2.5 V. Generally, in STS measurement, the feedback is off, and a low tunneling current indicates that little electronic information is captured. While in STM imaging, the feedback is on. Thus, when using a bias voltage corresponding to the low tunneling current in STS spectrum (such as in the wide gap region in Fig.3 (d)), the tip would approach the sample gradually, so the electronic information beneath the 2D lattices then may also be captured and overlay with the surface information. Because of the wide gap of the 2D Au lattices, the contrast in the STM images may not reflect the electronic structures of the 2D lattices. We suggest that it can be attributed to the electronic information beneath the 2D lattices, which originates from the interaction between the 2D lattices and the underlying substrate. However, this bias voltage-dependent morphology has not been observed in STM images with the Au coverage of 0.4 ML (not shown here). It may be ascribed to the strong interaction between Si substrate and the covered 1L Au-Si clusters, in which the electrons mainly transfer in the vertical direction. While in the 2D lattices, the in-plane coupling plays a significant role, so the transport of carriers in the lateral direction accounts for the major part compared with that in the vertical direction. No clear lateral transport behaviors is observed within the 2D Au lattices at -2.5 V, and the STM images exhibit an obvious asymmetry at the positive and negative bias voltage regions. This finding is consistent with our STS measurements in Fig. 3(b). For the 2D Au lattices, scanning at the positive or negative bias voltage implies the extraction or injection of electrons. Thus, the asymmetry may originate from

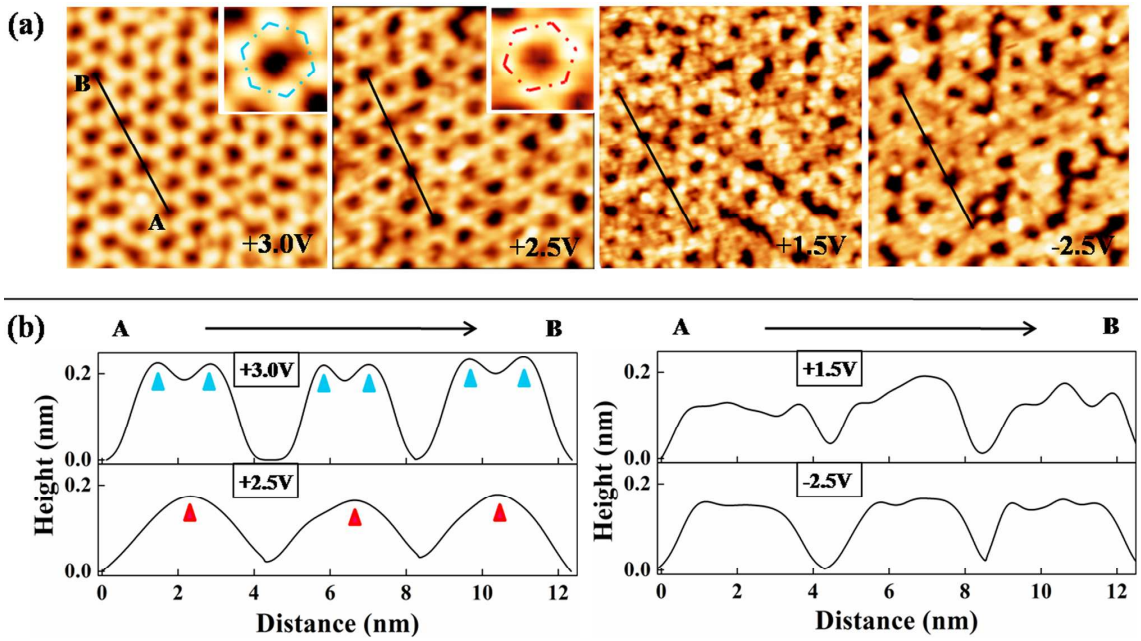

Fig. 4 (a) STM images (20×20 nm^2) of the 2D Au lattices on Si(111)-7×7 surface at the bias voltages of +3.0, +2.5, +1.5, -2.5 V. The hexagons in the insets outline the variation of morphology at different bias voltage; (b) the corresponding height profiles along line AB (marked on the STM images along Si <1 1 -2> orientation). The blue solid triangles at +3.0 V indicate the center of HUCs, while the red solid triangles at +2.5 V denote the site between HUCs (on the top of Si dimmers).

different types of carriers, *i.e.*, electron or hole. This uniqueness also suggests that the 2D lattices possess special carrier transport properties, which will be further discussed later.

Theoretical study for the unique transport preference and wide forbidden gap

In normal low-dimensional structures, Coulomb blockade and quantum size effect are usually used to explain the large energy gap in the I–V measurements.[25,26] For the typical Coulomb blockade and quantum size effect models, the gap should be decreased as their size is increased.[27] As to our case, these mechanisms can only explain the decreased energy gap as the individual Au_6Si_3 cluster grows into the 1L Au-Si layer, but failed to explain the obvious increased gap as the 1L Au-Si layer further grows to 2D Au lattices. As shown in Figure 5, for individual Au_6Si_3 cluster, the energy gap is about 1.9 eV (the inset shows its I-V and (dI/dV)/(I/V) curves with the data taken from our previous work in reference 12), which decreases to 1.0 eV when the Au coverage is increased to form the 1L Au cluster. Accordingly, if the Coulomb blockade or quantum size effect is still satisfied, an even narrower gap less than 1.0 eV (marked by the solid white square in Fig. 5) should be expected as the Au coverage is further increased to form the 2D lattices. However, the gap measured at 2D Au lattices is up to 4.1 eV, showing an opposite variation to the expected value. This fact suggests that the wide energy gap is not only induced by the LDOS of the 2D lattices, and could not be simply explained by the Coulomb blockade or quantum size effect. On the other hand, various-voltage STM studies reveal an in-plane coupling effect of the 2D lattices, indicating a potential barrier between the 2D lattices and beneath. Therefore, the electronic tunneling can be blocked in the vertical direction, and instead, has the preference in the lateral direction. In light of this finding, the wide energy gap more likely reflects the in-plane transport preference of the 2D Au lattices, where the electrons act as the De Brogile wave and transport in the lattices similar to the light in photonic crystal structures. Moreover, the coherence length of electron waves was estimated could be tens of nanometers at RT,[28] larger than the size of the grid points in our 2D Au lattices (about 1nm) and the distance between adjacent grid points (about 1.5 nm), which ensures the realization of wave nature of electrons in these 2D lattices. By this transport mechanism, the tunneling current may be blocked at

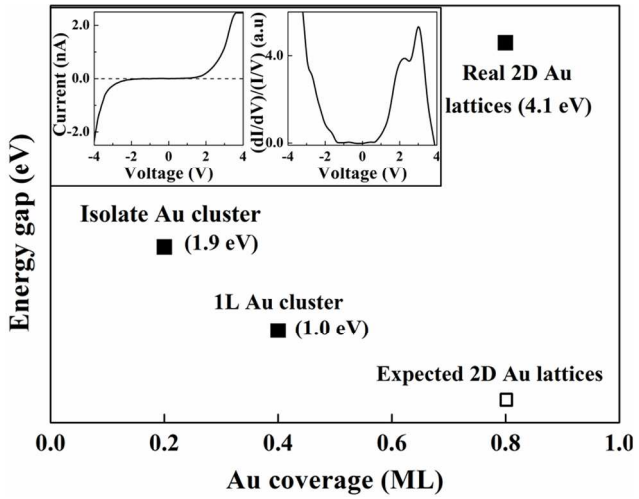

Fig. 5 Evolution of the energy gaps for different Au structures. The solid black squares present the energy gap obtained by STS measurements, and the solid white square presents the gap expected for 2D Au lattices by the normal size effect. Inset: I–V and corresponding normalized numerical differential curves for the individual Au_6Si_3 cluster.

certain bias voltage regions and modulated by the sixfold symmetrical periodic structure, inducing a forbidden gap in the (dI/dV)/(I/V) curve (Figure 4(d)).

To verify our speculations, the finite-difference time-domain method was employed to simulate the transport properties of the 2D Au lattices.[29] According to our STM observation, a honeycomb structure was designed with the shape of Au cluster in each HUC approximated as a cylinder, and the incident electron De Brogile wave was set in plane. The simulated wavelength spectrum is shown in Fig. 6(a), where the monitor value corresponds to the electron transport probability. The relation between electron wavelength and energy can be expressed as:

$$\lambda = \frac{h}{p} = \frac{h}{\sqrt{2m_0 E_k}} = \frac{hc}{\sqrt{2m_0 c^2 E_k}} \qquad (1)$$

where λ is the wavelength, h is Planck's constant, p is the momentum of electrons, m_0 is the static mass of electrons, E_k is the kinetic energy of electrons, and c is the speed of light. In a semiconductor, both electrons and holes are carriers, so the static mass of electrons should be substituted by the effective masses of electrons or holes. By adopting the above constants, the carrier transport probability can be described as the follow expression:

$$\lambda = \sqrt{\frac{m_0}{m_n^*}} \cdot \frac{1.226}{\sqrt{E_k(eV)}} = \sqrt{\frac{m_0}{m_n^*}} \cdot \frac{1.226}{\sqrt{U}} nm \qquad (2)$$

where U is the bias voltage and m_n^* is the effective mass of the carriers calculated from the equation:

$$E(k) - E(0) = \frac{h^2 k^2}{2m_n^*} \qquad (3)$$

where k is the wave vector in reciprocal space. The $E(k)$ relationship was obtained through the first-principles calculations (the band dispersion for the effective mass calculation is shown in supporting information S3), which gives the effective mass values of the electrons and holes to be about 0.55 m_0 and 0.26 m_0 in the 2D Au lattices, respectively. Accordingly, we suggest a possible electronic transport mechanism as follows. At positive voltages, the electrons are tunneled from the STM tip to the sample and then transport in the 2D Au lattices. Generally, the transport of electron wave decays rapidly when injected into the 2D lattices, especially for electrons with low energy (large electron wavelength). Only when the energy of electrons reaches a certain value, the electron wave could transport in a certain region. Except for the electron energy, transport probability could be further modulated by the symmetry of 2D lattices, which may be the reason for the fluctuation of the transport probability in Fig. 6(a). By employing the electron effective mass, the bias voltage dependent transport probability at the positive voltage region was calculated and shown in Fig. 6(b). At voltages higher than +1.3 V, electrons have a high transport probability in the 2D lattices, while at voltages between 0 and +1.3 V, the probability steeply drops to almost zero, leading to a transport block. As a result, a transport gap from approximately 0 V to +1.3 V could be

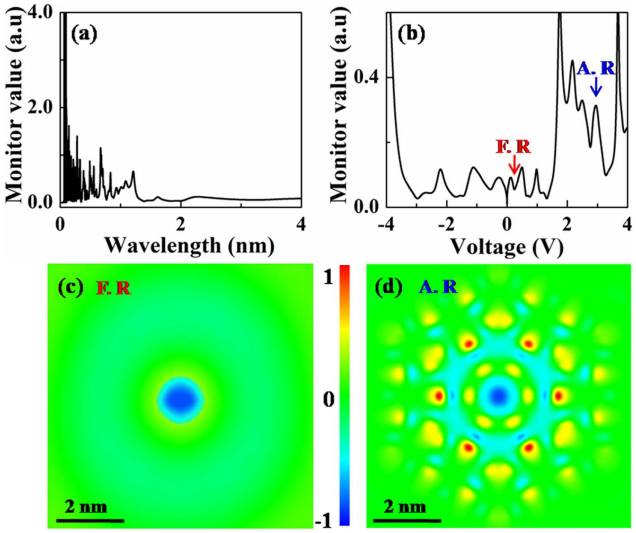

Fig. 6 (a) The simulated wavelength-dependent transport probability of electrons in the 2D Au lattices, where the electron De Brogile wave was set propagating within the plane; (b) The bias voltage-dependent transport probability of both the electrons and holes; (c) And (d), the probable distribution of the electron transporting in the 2D lattices, with the voltages were set at +0.3 V (F. R (forbidden region for carrier transport)) and +3.0 V (A. R (available region for carrier transport)), respectively.

observed when measuring the electronic properties of the 2D Au lattices. Similarly, at negative voltages, electrons tunnel from the sample to the STM tip, and equivalently, the holes transport in the 2D Au lattices. By adopting the calculated effective mass of the holes, the voltage dependent transport probability for the holes also exhibits an obvious transport gap from about 0 to -3.0 V. The different effective masses between the electrons and holes explain the asymmetry of the energy gap around the Fermi level. The total energy gap from approximately -3.0 V to +1.3 V in the simulated spectrum agrees well with the STS measurements in Fig. 3(d). This agreement inspired us that the wide energy gap measured by STS more likely originates from the carriers transport properties in the 2D Au lattices. Thus, the electronic structures may be affected by carrier transport behaviors in 2D lattices. To further understand the transport route of carriers in these 2D lattices, the distribution of electrons at two different voltages, one of +0.3 V, in the forbidden gap that unavailable for electron transport, and the other of +3.0 V, out of the gap that available for electron transport, are displayed in Fig. 6(c) and 6(d), respectively. At +0.3 V, the electrons are mainly confined in the central region, *i.e.*, around the tip, indicating that the electrons could not transport outward. At +3.0 V, the electrons spread out obviously and show sixfold symmetric poles, which are consistent with the honeycomb structures. These facts suggest that the carrier transport behaviors are modulated by the symmetry of 2D Au lattices, and the transport blocking at lower bias voltage regions may be responsible for the generation of the wide forbidden gap. As a new found system, a completely understanding of the 2D Au lattices needs much more experimental and theoretical studies, which will be further pursued in our future work.

Conclusions

In summary, large-area 2D Au lattices are successfully fabricated by the deposition of 0.8 ML Au atoms onto clean Si(111)-7×7 surface. First-principles calculations combined with RHEED and STM images reveal that the 2D Au lattices compose two interfacial distinct 1L and 2L layers which are completely formed one after another without intergrowth. Au atoms in 2L layer are directly located on top of the 1L Au-Si layer, forming the close-packed structure. Bias-dependent STM images show an interesting Kagome-like distribution of electronic states due to the electronic coupling effect. As a result, the carriers can transport in 2D Au lattices, which induces a special modulation to the electronic structures, leading to an abnormal wide energy gap from -3.0 to +1.1 V in STS measurements. Theoretical simulations suggest that the unique transport preference is determined both by the carrier energy and the symmetry of 2D lattices. And the calculated forbidden gap from -3.0 to +1.3 V is well agreed with the STS result. Within the gap, the carriers are confined around the tip, while out of the gap, the carriers will transport outward with a 2D diffraction of carrier waves by the standing field. Therefore, aside from the electronic states, the transport behavior of carriers also contributes to the electronic structures of 2D Au lattices. Results of this study provide insights into the growth mechanism and the unique transport preference of artificial 2D lattices, which may serve some references for the controlled fabrication and for routing the carrier transport behavior of low-dimensional structures.

Acknowledgments

This work is financially supported by the National "973" Program of China (Grant Nos. 2011CB925600, and 2012CB619301), the National Natural Science Foundation of China (Grant Nos. 61227009, 91321102, 11304257, and 11104229), and the Natural Science Foundation of Fujian Province of China (Grant No: 2014J01026).

Notes and references

Department of Physics, Fujian Key Laboratory of Semiconductor Materials and Applications, Xiamen University, Xiamen, 361005, China. Tel: 86-592-2185962; E-mail: ypwu@xmu.edu.cn, yhzhou@xmu.edu.cn or jykang@xmu.edu.cn

1. Y.-F. Liu, K. Krug, and Y.-L. Lee, *Nanoscale.*, 2013, **5**, 7936.
2. Y. Wu, Y. Hao, H. Y. Jeong, Z. Lee, S. Chen, W. Jiang, Q. Wu, R. D. Piner, J. Kang, and R. S. Ruoff, *Adv. Mater.*, 2013, **25**, 6744.
3. X. Zhang, S. Wang, Y. Shen, Y. Guo, Q. Zeng, and C. Wang, *Nanoscale.*, 2012, **4**, 5039.
4. Y. Zang, X. He, J. Li, J. Yin, K. Li, C. Yue, Z. Wu, S. Wu, and J. Kang, *Nanoscale.*, 2013, **5**, 574.
5. H. Qin, Y. Gao, J. Teng, H. Xu, K. Wu, and S. Gao, *Nano Lett.*, 2010, **10**, 2961.
6. T. Zhang, P. Cheng, W.-J. Li, Y.-J. Sun, G. Wang, X.-G. Zhu, K. He, L. Wang, X. Ma, X. Chen, Y. Wang, Y. Liu, H.-Q. Lin, J.-F. Jia, and Q.-K. Xue, *Nat. Phys.*, 2010, **6**, 104.
7. J. G. Analytis, R. D. McDonald, S. C. Riggs, J.-H. Chu, G. S. Boebinger, and I. R. Fisher, *Nat. Phys.*, 2010, **6**, 960.
8. Y. Jiang, Y. N. Zhang, J. X. Cao, R. Q. Wu, and W. Ho, *Science.*, 2011, **333**, 324.
9. G. Li, P. Höpfner, J. Schäfer, C. Blumenstein, S. Meyer, A. Bostwick, E. Rotenberg, R. Claessen, and W. Hanke, *Nat. Commun.*, 2013, **4**, 1620.
10. J.-F. Jia, X. Liu, J.-Z. Wang, J.-L. Li, X. Wang, Q.-K. Xue, Z.-Q. Li, Z. Zhang, and S. Zhang, *Phys. Rev. B.*, 2002, **66**, 165412.
11. C. Zhou, Q. Xue, J. Jia, H. Zhan, and J. Kang, *J. Chem. Phys.*, 2009, **130**, 024701.
12. Y. Wu, Y. Zhou, C. Zhou, H. Zhan, and J. Kang, *J. Chem. Phys.*, 2010, **133**, 124706.
13. H. Raza, T. Raza, and E. Kan, *Phys. Rev. B.*, 2008, **78**, 193401.
14. S. Yamazaki, I. Matsuda, H. Okino, H. Morikawa, and S. Hasegawa, *e-Journal Surf. Sci. Nanotechnol.*, 2005, **3**, 497.
15. J. Kierfeld and V. Vinokur, *Phys. Rev. B.*, 2004, **69**, 024501.
16. D. W. Prather, S. Shi, J. Murakowski, G. J. Schneider, A. Sharkawy, C. Chen, and B. Miao, *IEEE J. Sel. Top. Quantum Electron.*, 2006, **12**, 1416.
17. H. Masuda, M. Yamada, F. Matsumoto, S. Yokoyama, S. Mashiko, M. Nakao, and K. Nishio, *Adv. Mater.*, 2006, **18**, 213.
18. Y. Zhou, Q.-H. Wu, C. Zhou, H. Zhang, H. Zhan, and J. Kang, *Surf. Sci.*, 2008, **602**, 638.
19. H. Chang, M. Lai, J. Wei, C. Wei, and Y. Wang, *Phys. Rev. Lett.*, 2004, **92**, 066103.
20. R. Feenstra, *Phys. Rev. B.*, 1994, **50**, 4561.
21. S. Hu, A. Zhao, E. Kan, X. Cui, X. Zhang, F. Ming, Q. Fu, H. Xiang, J. Yang, and X. Xiao, *Phys. Rev. B.*, 2010, **81**, 115458.
22. Z.-X. Xie, K. Iwase, T. Egawa, and K. Tanaka, *Phys. Rev. B.*, 2002, **66**, 121304.
23. Q. Chen, S. C. Bae, and S. Granick, *Nature.*, 2011, **469**, 381.
24. M. Bayer, P. Hawrylak, K. Hinzer, S. Fafard, M. Korkusinski, Z. R. Wasilewski, O. Stern, and A. Forchel, *Science.*, 2001, **291**, 451.
25. L.-P. Xu and S. Chen, *Chem. Phys. Lett.*, 2009, **468**, 222.
26. S. Kano, Y. Azuma, M. Kanehara, T. Teranishi, and Y. Majima, *Appl. Phys. Express.*, 2010, **3**, 105003.
27. Y. Jiang, K. Wu, J. Ma, B. Wu, E. Wang, and P. Ebert, *Phys. Rev. B.*, 2007, **76**, 235434.
28. T. Hiramoto, K. Hirakawa, Y. Iye, and T. Ikoma, *Appl. Phys. Lett.*, 1989, **54**, 2103.
29. B. Fain, I. Robert-Philip, a Beveratos, C. David, Z. Z. Wang, I. Sagnes, and J. C. Girard, *Phys. Rev. Lett.*, 2012, **108**, 126808.